Untreated bamboo biochar as anode material for sustainable lithium ion batteries

Biomass and Bioenergy 193 (2025) 107511

Contents lists available at ScienceDirect

Biomass and Bioenergy

journal homepage: www.elsevier.com/locate/biombioe

Untreated bamboo biochar as anode material for sustainable lithium ion batteries

Mario Junior Barbosa Nogueira [a], Susana Chauque [b], Valeria Sperati [b,c], Letizia Savio [d], Giorgio Divitini [b], Lea Pasquale [b], Sergio Marras [b], Paola Franchi [e], Sidnei Paciornik [a], Remo Proietti Zaccaria [b], Omar Ginoble Pandoli [b,f,g,*]

[a] Departamento de Engenharia Química e de Materiais, Pontifícia Universidade Católica do Rio de Janeiro (PUC-Rio), Rua Marquês de São Vincente, 225, 22451-900, Rio de Janeiro, Brazil
[b] Istituto Italiano di Tecnologia (IIT), Via Morego 30, 16163, Genova, Italy
[c] GAME Lab, Department of Applied Science and Technology, Politecnico di Torino, Corso Duca degli Abruzzi, 24, 10129, Turin, Italy
[d] Istituto dei Materiali per l'Elettronica e il Magnetismo del Consiglio Nazionale delle Ricerche, UOS Genova, Via Dodecaneso 33, Genova, Italy
[e] Department of Chemistry "Giacomo Ciamician", University of Bologna, Via P. Gobetti 85, 40129, Bologna, Italy
[f] Departamento de Química, Pontifícia Universidade Católica do Rio de Janeiro (PUC-Rio), Rua Marquês de São Vincente, 225, 22451-900, Rio de Janeiro, Brazil
[g] Dipartimento di Farmacia, Università degli Studi di Genova, Viale Cembrano 4, Genova, Italy

ARTICLE INFO

Keywords:
Bamboo-based biochars
Monolithic carbon
Slow pyrolysis
EPR
Permanent free radicals
Lithium battery

ABSTRACT

Biochar, a carbon-rich material derived from lignocellulose biomass through pyrolysis, is being considered for lithium-ion battery (LIB) applications due to its sustainable sourcing, manufacturing, and favourable electrochemical properties. A biochar-based anode is a greener alternative to conventional materials, potentially reducing the environmental and financial costs of LIB production. Minimizing cost and simplifying the manufacturing process for LIBs drive the development of new scalable production of plant-based products to create greener anodes for lithium batteries. In this work, bamboo-based biochar (BCs) was prepared through an optimized slow pyrolysis route with two thermal treatments at 800 °C (B800) and 1000 °C (B1000), and used as a LIB anode. Compared to B1000, B800 presented higher *d*-spacing (d_{002} = 0.3657 nm) and graphitic crystallite size (L_a = 13.8 nm), smaller pore sizes (38 Å) with higher surface area (310 m^2/g), and a higher concentration of permanent free radicals (PFRs) centered on the carbon (1.85 × 10^{18} spin/g). Although B1000 is slightly more conductive than B800, the physicochemical properties of B800 could enhance the lithiation of the pseudographitic structures and facilitate the reduction of Li^+ ions due to the presence of PFRs. The half-cell LIB using B800 presented a reversible capacity of about 250 mA h/g at C/5 and long-term stability up to 450 cycles. This study highlights the potential of bamboo-based biochar as a viable and environmentally friendly anode material for the next generation of high-performance LIBs.

1. Introduction

The ever-growing demand for energy storage must be managed by engineering solutions that enable scalability while controlling their total environmental footprint. The carbon anode material represents a significant fraction of the total weight of a battery and has a substantial weight on the overall materials footprint of a device. Biomass-based carbons (biochars, BC) as anodes for sustainable lithium- [1], sodium- [2], and potassium-ion batteries [3] (LIB, NaIB, KIB) [4] have been explored as abundant, renewable, and low-cost resources to address the big issue of graphitic carbons' scalability production to supply the HEV/EV industry [5,6]. The biochar's properties, production cost, and environmental impact depend on the raw biomass sources and the carbonization methods [7]. To tune the physicochemical properties of plant-derived carbons to improve carbonaceous anodes' electrochemical performance, pre- and post-treatment for chemical modifications and/or physical activations have been employed. These additional processes will increase the cost of BC.

The redox properties of plant biomass-derived biochar with permanent free radicals (PFRs) have electrochemically been characterized

* Corresponding author. Istituto Italiano di Tecnologia (IIT), Via Morego 30, 16163, Genova, Italy.
E-mail addresses: omarpandoli@puc-rio.br, omar.ginoblepandoli@unige.it, omar.ginoble@iit.it (O. Ginoble Pandoli).

https://doi.org/10.1016/j.biombioe.2024.107511
Received 19 September 2024; Received in revised form 21 November 2024; Accepted 21 November 2024
Available online 3 December 2024

[8–10]. More recently, the electron-accepting (EAC) and electron-donating (EDC) capacity of wood-based biochars pyrolyzed at different treatment temperatures (TT) have attracted attention for several applications in redox-mediated reactions [9]. Less attention has been paid to the potential impact of reducing Li^+ ions during the intercalation into the pseudographitic domain of the BC. The reversible intercalation mechanism of metal alkaline ions into randomly oriented pseudographitic sheets of higher plant-derived BC, as well as the absorption phenomena of the metals in surface edges, active sites, heteroatoms (N, P, S, B, etc.), defects and nano/micro/mesopores, is still a scientific debate [4].

Bamboo is a giant grass as a potential bioenergy feedstock [11]. It is a gradient functional material with highly oriented lignocellulose polymers distributed to protect the living cells (parenchyma tissue), and the lignified sclerenchyma fibers are devoted to protecting the vascular bundle system [12,13]. It has already been used for applications in energy devices applications [14]: as supercapacitors [15–19], electrodes for solar cells [20], and green anode electrodes for batteries [21–29]. Bamboo is an anisotropic material [30–32] that has already bioinspired several nanotechnology applications [33,34] and sustainable bio-devices [34]. It is a promising natural 3D template for chemical [35,36] and electrochemical biobased devices (*bambootronic systems*) [37] that takes advantage of its hierarchical architecture, vascular bundles microfluidic system, high content of crystalline cellulose, and mechanical and electrical anisotropic properties [38,39]. A novel resistive three-dimensional carbonaceous material (3D-CM, $\sigma = 6.6$ S/m) was obtained with a low thermal treatment at 700 °C and used as continuous 3D microfluidic heaters exploring a Joule effect when a direct current to the 3D-CM is applied. Increasing the thermal treatment up to 1000 °C made it possible to modulate the monolithic conductive electrode sensors' electric properties ($\sigma = 250$ S/m) [40]. Recently, the production of bamboo-based biochar with different PFR contents has been demonstrated to be a pivotal contribution to organic dye removal from water solution by an electron transfer mechanism [41]. In this context, there is not yet evidence about the contribution of PFR on anode carbonaceous material applied in lithium-ion batteries.

Herein, we disclosed a sustainable, environmentally friendly, and low-cost conductive biochar obtained from highly oriented crystal lignocellulosic imbibed into the hierarchical structure of bamboo. We used slow pyrolysis treatment at 800 °C (resulting in the material labelled B800) and 1000 °C (B1000) to obtain monolithic conductive carbon without any pre- and post-treatment of the pyrolytic product from a pristine Bamboo *Dendrocalamus giganteus* species. Bamboo-based biochar (BCs) B800, compared to B1000, was tested as an anode in LIBs with a better reversible capacity of about 250 mA h/g maintained for up to 450 cycles.

2. Experimental section

2.1. Sample preparation

Bamboo biochar carbons (BC) were produced from 4-year-old Giant bamboo (*Dendrocalamus giganteus*) cut 2 m away from the root at the PUC-Rio campus, Brazil [39,42–44]. The pyrolysis procedure consisted of a thermal treatment under N_2 atmosphere at two different final temperatures, i.e., 800 and 1000 °C was fully described previously [40]. Hereafter, the samples are named B800 and B1000, respectively. The monolithic bulk materials B800 and B1000 were used for electrical impedance measurement, Raman spectroscopy, X-ray fluorescence (XRF) mapping, and X-ray Photoelectron Spectroscopy (XPS). The bulk pyrolyzed bamboo was ground with a Retsch MM 400 ball mill with a total collision time of 30 min and a frequency of 15/s. The powdered materials used to assemble the half-cell coin were analyzed by X-ray powder diffraction (XRPD), electron paramagnetic resonance (EPR), inductively coupled plasma-optical emission spectrometry (ICP-OES), scanning electron microscopy (SEM-EDX), and Brunauer-Emmett-Teller (BET) analysis. For a complete characterization of bamboo-derived carbons by electron paramagnetic resonance (EPR) [41], elemental chemical analysis, thermogravimetric analysis (TGA), μ-CT, HR-TEM, and thermoelectric characterization, the reader is directed to Ref. [40].

2.2. Bamboo bulk and biochar chemical-physical characterization

Electrochemical Impedance Spectroscopy (EIS) of bulk samples B-800 and B-1000 with 1 cm^3 were connected longitudinally to the sclerenchyma fibers using copper foils on steel plates and mounted in custom testing apparatus, allowing control of the electrical measurements using four-terminal sensing. A frequency response analyzer (SI 1260 Electrochemical Interface, Solartron Analytical, Farnborough, UK) was used to carry out the EIS measurements by applying a 10 mV AC signal in the 1 KHz– 1 MHz frequency range [45]. Raman spectroscopy analysis of the thermally treated bamboo was performed with a confocal Raman microscope (HORIBA Jobin-Yvon, model XploRA) at an exciting wavelength of 532 nm. X-ray fluorescence (XRF) mapping multi-element analysis was performed by Tornado M4 Micro X-ray fluorescence. The fundamental parameters equation provided the relative quantification. X-ray photoemission spectroscopy (XPS) experiments were performed in a dedicated ultra-high vacuum (UHV) chamber at a base pressure of $5{\cdot}10^{-8}$ mbar, using a hemispherical analyzer model 10–360 and a monochromatic X-ray source model 10–610 by Physical Electronics. Slices of pyrolyzed bamboo were introduced into the chamber through a fast entry lock system, after outgassing in the pre-chamber for more than 24 h. Such a long time is due to the channel structure of the material, implying a high specific surface. XPS spectra were acquired using monochromated $Al_{K\alpha}$ photons of energy $h\nu = 1486.6$ eV from a spot of approximately 100 μm diameter and analyzed using the KolXPS software. Binding energies were calibrated by setting the maximum C 1s line to 284.5 eV and cross-checking that the corresponding O 1s binding energy agrees with values previously reported in the literature [40,46–48].

The C 1s region is fitted with a Doniach-Sunjic component convoluted with a Gaussian and minor additional Voigt components in the high-energy tail. The O 1s region is fitted with up to 4 Voigt lines, while only two were sufficient to reproduce the weak N 1s intensity. Peak areas are affected by an error of ±5 %. For a quantitative evaluation of the relative elemental concentration, the fitted C 1s and O 1s areas must be weighted for the corresponding atomic sensitivity factor (ASF - taking into account the photoemission cross section and the transmission function of the analyzer), which is 2.4 times larger for O 1s than for C 1s under the present experimental conditions [49].

XRD patterns from 10° to 70° were collected in Parallel Beam (PB) geometry, using a third-generation Empyrean diffractometer (Malvern-PANalytical, Westborough, MA) equipped with a 1.8 kW CuKα X-ray source operating at 45 kV and 40 mA, automated prefix iCore-dCore optical modules for the incident and diffracted beam paths, 0.28° parallel plate collimator (indicated for analysis on samples with irregular shape and high surface roughness) PIXcel^{3D} area detector. Measurements were conducted at room temperature in an ambient atmosphere using a zero-diffraction silicon sample holder. Data analysis was performed with HighScore Plus v. 5.2 software.

The Brunauer-Emmett-Teller (BET) analysis was carried out to determine the bamboo biochar's surface area and pore diameter. The N_2 adsorption-desorption isotherms were obtained at 77 K.

Electron paramagnetic resonance (EPR) spectra were recorded by a Bruker ELEXSYS E500 spectrometer equipped with an NMR Gaussmeter to calibrate the magnetic field and a frequency counter to determine g-factors. Measurement conditions: modulation amplitude = 1.0 G; conversion time = 81.92 ms; time constant = 81.92 ms; modulation frequency = 100 kHz; field width = 100 G, microwave power = 0.80 mW; and microwave frequency = 9.30 GHz.

The morphology of the biochar and the anode slurries was observed using scanning electron microscopy (SEM) images acquired on a ZEISS

GeminiSEM 560 operated at 2 kV. The signal was collected using the in-lens secondary electron detector. EDX data were collected at 20 kV acceleration voltage using an Oxford Instruments X-max detector and processed within Inca.

2.3. Electrode and coin-cell preparation

The bamboo biochar-based anodes were fabricated using conventional slurry preparation and doctor-blade coating. The anode slurry was prepared by mixing B800 and B1000 active materials, Super P carbon (from Imerys, Graphite & Carbon, Willebroek, Belgium) as a conductive agent, and polyvinylidene difluoride (PVdF), from Solvay, Bollate, MI, Italy) as a binder in 80:10:10 wt ratio using N-methylpyrrolidone NMP (from Sigma Aldrich, Merck Life Science S. r.l., Milano, MI, Italy) as solvent. The homogeneous mixture was cast onto a copper foil (15 μm of thickness) current collector using the doctor-blade method and dried overnight at room temperature. The electrode foil was punched into 12 mm diameter disks, dried under vacuum at 80 °C overnight, and transferred in an argon-filled glovebox for the coin half-cell assembly. The final active mass loading of the bamboo anodes was 1–2 mg/cm^2. As an electrolyte, it employed the LP30 commercial solution (1M $LiPF_6$) in a solvent mixture of 1:1 w/w of ethylene carbonate (EC) and dimethylene carbonate (DMC). The amount of electrolyte was kept constant at 100 μL for all the fabricated cells.

2.4. Electrochemical testing and characterization of bamboo-based anodes

The electrochemical performance of the bamboo biochar-based anodes was tested in CR2032-coin half cells, formed by lithium chips used as counter and reference electrodes, a glass fiber working as a separator, and the B800 and B1000 slurry as the working electrode. The assembling process was carried out in an MBraun glovebox with water and oxygen levels lower than 0.1 ppm. The electrochemical characterization was performed in duplicate using a BCS–805 multichannel battery unit from BioLogic (BioLogic, Seyssinet-Pariset, France). For the half-cell analyses, a constant current (CC) protocol at C/5 was used for long cycling and rate capability (C/5, C/2, 1C, 2C, 4C, 10C, and C/5 again) tests. To calculate the C-current value, we referred to H. Darjazi et al. work, where the 1C value is defined as 300 mA/g [50,51]. Furthermore, cyclic voltammetry (CV) measurements were performed at 0.1 mV/s. The potential range in all the electrochemical measurements was 0.01–3.00 V vs Li/Li$^+$.

3. Results and discussion

The electrical conductivity of pyrolyzed bulk bamboo was fully demonstrated previously, indicating a direct dependence on several physical and chemical parameters from the raw lignocellulosic material to the carbon products: highly oriented crystallinity of cellulose fibers, graphitization degree, volume shrinkage with higher contact of the carbon crystallite domains, density, intraparticle conductivity, C/H elemental composition, and surface chemistry [40]. In Fig. 1, electric impedance measurements for the bulk samples B-800 and B-1000 along the longitudinal alignment of carbon domains demonstrate an electric conductivity independent of the applied frequency. This electric response is characteristic of a carbon material with a total percolation state with a direct-current (DC) conductivity, as observed by Nagle et al. [40,52]. The electric conductivities parallel to the fiber of the two samples are similar, 102 and 112 S/m, for B-800 and B-1000, respectively. In the trade-off between total manufacturing cost and performance, the negligible difference in electrical conductivity could justify the economic and environmental advantages of saving time, energy, and other additives to obtain a conductive material at lower temperatures without chemical/physical treatments of raw lignocellulose biomass.

Tables S1 and S2 summarize the chemical composition [wt%] of the bamboo pyrolyzed powder (B800 e B1000) determined by ICP-EOS analysis. For the ICP-EOS quantitative analysis, the pulverized samples were treated with HNO_3 to extract about 1.5 % w/w of metal ions. The most representative metals extracted (Ca, K, Mg, P, Na, and S) were below 0.3 %, which did not influence the electric conductivity of the monolithic carbon material [40]. A semi-quantitative XRF analysis of bamboo bulk confirmed the ICP-EOS analysis (Tables S3 and S4). The XRF mapping analysis of the bulk pristine bamboo and B800 sample in the transversal and longitudinal sections revealed a different chemical distribution of metal ions (Figs. S1–S4). On the transversal surfaces, for all the regions of interest (ROI: external, middle, and internal), S, P, and Ca are more concentrated in parenchyma tissue, K in the sclerenchyma fibers, while Mg is ubiquitous in both tissues. In Fig. S5, the XRF mapping along the longitudinal section reveals an alternating stratification of the metals into the parenchyma, sclerenchyma, and internal channels.

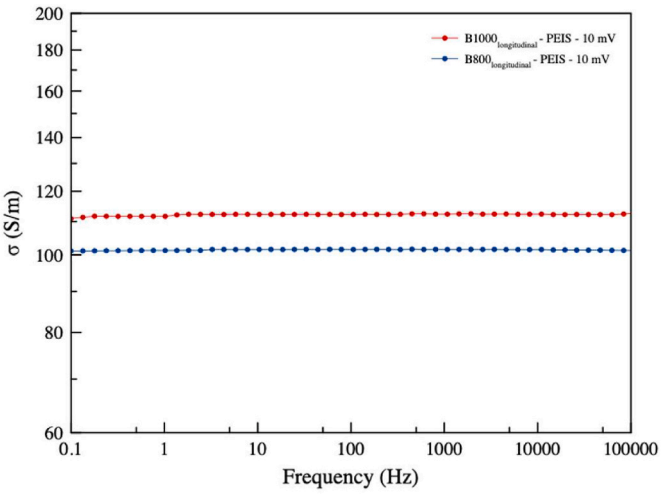

Fig. 1. Electric conductivity (S/m) from 1 KHz to 1 MHz for bulk samples (B-800 and B-1000) parallel to the uniaxially-aligned fibers.

To study the graphitization process with two distinct treatment temperatures (800 and 1000 °C), bamboo samples were analyzed by Raman spectroscopy. In Fig. 2, Raman spectra of B-800 and B-1000 recorded from 800 to 3200 cm^{-1} show the disorder-induced D band at 1332 cm^{-1}, the G-band at 1530 cm^{-1} and the second-order bands, namely the 2D band at 2730 cm^{-1} and the D + D′ band at 2915 cm^{-1}. The degree of disorder in carbon materials has been widely ascertained

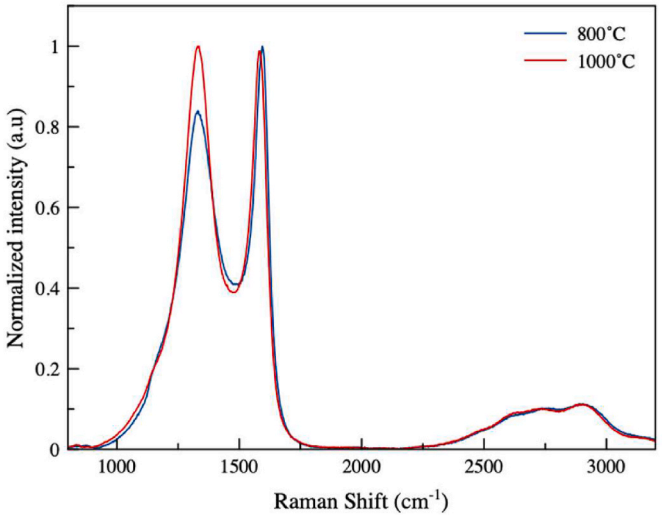

Fig. 2. Raman characterization of bamboo biochar obtained at different temperatures.

by analyzing the intensity ratio of the D and G bands, I_D/I_G. There is an initial stage of carbon graphitization where amorphous carbon turns into nanographite, and the I_D/I_G ratio rises. In this instance, the I_D/I_G ratio rises from 0.85 for B800 to 1.0 for B1000, whereas graphitic crystallite size (L_a) decreases from 13.8 nm to 12.7 nm. The complete interpretation of the evolution of cellulose to carbons during the carbonization process and the determination of the graphitic crystallite size (L_a) have already been described previously [40].

The increase of the I_D/I_G could be related to a higher defectivity of the smaller graphene-like domains typical for thermally reduced graphite oxide (rGO) [53–56]. These additional defects could be then saturated by organic volatile contaminants when the system is exposed to air. Coherently, a weak component at binding energy BE = 289.8 eV appears in the high-resolution XPS spectra, as discussed later.

Fig. 3 shows the XPS spectra of the B800 and B1000 samples with the main elements present at the surface. The C 1s region presents a main, graphite-like C 1s line at 284.5 eV, and a small contribution of oxygenated carbon at higher BE for the B1000 sample. The shape of the peak is in perfect agreement with the one previously observed for pyrolyzed bamboo powders and confirms that the surface consists of C atoms in sp^2 hybridization [40]. As already mentioned, the small 289.8 eV and 291.1 eV lines present in the B1000 spectrum are typical of C bound to O atoms; they suggest a small surface contamination by organic species and by Cl, as revealed also by the weak Cl 2p intensity appearing in the survey spectrum.

Finally, the 293.6 eV peak corresponds to the K 2s line and confirms the presence of potassium in this sample, as already apparent from the survey. The O 1s peak consists of up to 4 components related to the organic contaminants already detected in the C 1s spectra and to possible OH adsorption. Considering the different atomic sensitivity factors of C 1s and O 1s under the present measuring conditions, we estimate a C/O ratio of (8.8 ± 0.9) and of (10.5 ± 1.0) for B800 and B1000, respectively, in good agreement with the value of (7.5 ± 0.7) previously found for a powdered B1000 sample [40]. The slightly lower oxygen content detected for the sliced sample compared to the powdered one can be explained in terms of the lower specific surface of the analyzed spot. Finally, the N 1s intensity is negligible for B1000, whereas for B800, it is only reminiscent of the nitrogen content present in the original material. Despite that, two inequivalent N 1s species are evident. The heteroatoms N could be involved in Li-ion binding during the intercalation-adsorption mechanism.

The bamboo samples were analyzed using powder X-ray diffraction (PXRD). Fig. 4 shows the XRPD patterns of the bamboo samples treated at 800 and 1000 °C, and Table 1 summarizes XRD patterns' data. The broad (002) band at an angular position higher than 2θ = 24° indicates a high degree of graphitization, while the reflection observed at around 2θ = 43° is characteristic of a carbon phase with a two-dimensional turbostratic structure. B800 presents the (002) diffraction peak at lower angles and broader FWHM, indicating higher interplanar d-spacing d_{002} (3.657 Å vs 3.633 Å) and crystalline domains smaller than the B1000 XRD pattern. These values are much greater than that of graphite (3.350 Å). Increasing the d-spacing could facilitate the intercalation between the graphitic layers of the lithium cation with an ionic radius of 0.76 Å.

However, we can suppose the tandem mechanism intercalation-adsorption already revealed for hard carbons (or non-graphitizable carbons) [4]. The adsorption of Li ions might result from the metal ions' insertion into the defect sites confirmed by the Raman D band, mesopores, amorphous carbon regions, or binding with residual N heteroatoms. The mechanism of the intercalation of alkali metals into hard carbons is still controversial and beyond the scope of this study. With nitric acid digestion, we quantify 1,5 % w/w of metal inside the pyrolyzed bamboo (Table S1). XRF mapping and ICP-EOS analysis of the bulk sample confirmed the most abundant metal (Tables S1–S3 and Figs. S1–S4). As demonstrated, the electric conductivity is minimally affected by the presence of the metal ions [33], and we decided to avoid any chemical treatment of the biochar to optimize time consumption and cost and minimize waste.

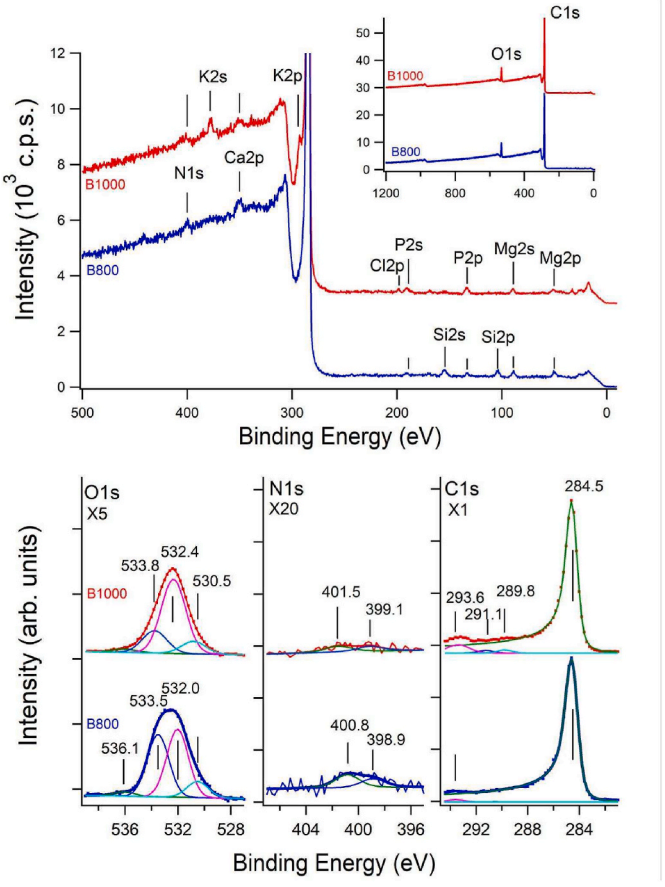

Fig. 3. (Upper panel) XPS spectra of the B800 and B1000 samples showing the main elements present at the surface. The inset reports the survey spectra, recorded in the full BE range and showing that the main surface element is C, followed by O. The main panel shows an enlargement in the (500; 0) eV energy range that allows to appreciate the presence of other elements in much smaller amount. (Bottom panel) High-resolution XPS spectra of O 1s, N 1sa and C 1s regions for the B800 and B1000 samples. The outcome of the fitting procedure and the different components identified for each spectrum are reported. Note the magnification factor on each panel.

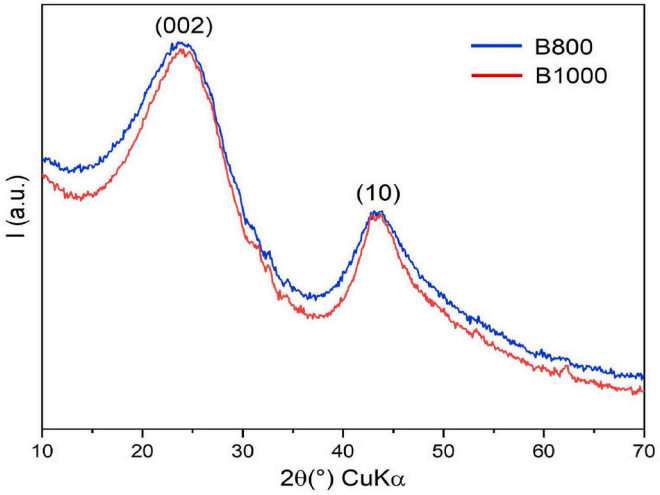

Fig. 4. XRPD analysis of biochars (B800 and B-1000).

Table 1
Data analysis of XRPD patterns of pyrolyzed bamboo samples.

Sample	2θ° (002)	FWHM (°) (002)	d-spacing (Å) d_{002}	(2θ°) (10)	FWHM (°) (10)
B800	24.322	8.706	3.657	43.256	7.037
B1000	24.481	8.471	3.633	43.138	6.070

The BET analysis was performed to determine the evolution of the surface area and pore size during the thermal treatments. Data plotted in Fig. 5 show a decrease in the surface area from 310 to 125 m^2/g, while the pore size increases from 38 to 72 Å, respectively, from B800 to B1000. This evidence will explain the best electrochemical performance of the B800-anode compared to the B1000. Smaller pore sizes with higher surface area could improve the lithiation and ions intercalation into the B800 biochar [4]. For both samples, the isotherm absorption of N_2 profiles indicates the presence of the mesopores (pore size ranging between 2 and 50 nm) (Fig. S6).

Fig. 6 and Table 2 show the results of EPR analyses. The presence of permanent free radicals (PFRs) revealed that the concentration of paramagnetic centres in the bamboo samples depends on the pyrolysis temperature [41]. In particular, the presence of PFRs was significant in B800 (1.85×10^{18} spins/g), while it became irrelevant in B1000 (3.40×10^{15} spins/g). The loss in EPR signal is due to the recombination of the radical species during the graphitization process, as evidenced by the DRX profile (Fig. 4). These results follow other woody lignocellulosic biomass under different pyrolysis biomass [57]. According to the literature, the g-factor value of around 2.0029 was mainly consistent with sp^2 aromatic π-radicals [58]. This finding suggests that B800 is a more efficient electron acceptor for lithium, accommodating a large amount of Li-ion during the intercalation and reduction into the anode carbon material [59]. In the future, *in-situ* EPR studies monitoring alkali metal's lithiation/delithiation process will be necessary to understand the electron transfer of rechargeable batteries [60–62].

As described in the experimental section, we prepared a carbon-based slurry using bamboo biochar as an electrode material for the LIB anode. The SEM images of the bamboo-based slurry are presented in Fig. 7. The biochar presents an overall inhomogeneity of particles in the slurry for both samples. In Figs. S7–10, the EDX 2D mapping shows the chemical composition of several elements uniformly distributed onto the surface. After electrochemical cycling, inevitable changes are observed to the fine structure. In Fig. S11, are shown SEM images from the B800 and B1000 samples before and after electrochemical testing.

3.1. Performance of bamboo-based biochar negative electrode in LIBs

The storage of lithium and sodium in biochar-based materials

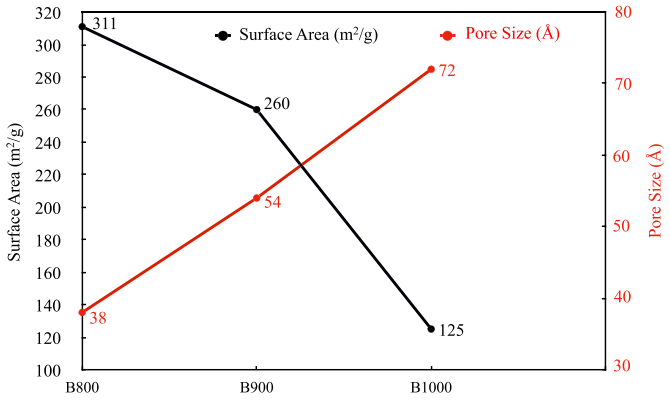

Fig. 5. BET analysis of the bamboo biochar after different temperature treatments during pyrolysis.

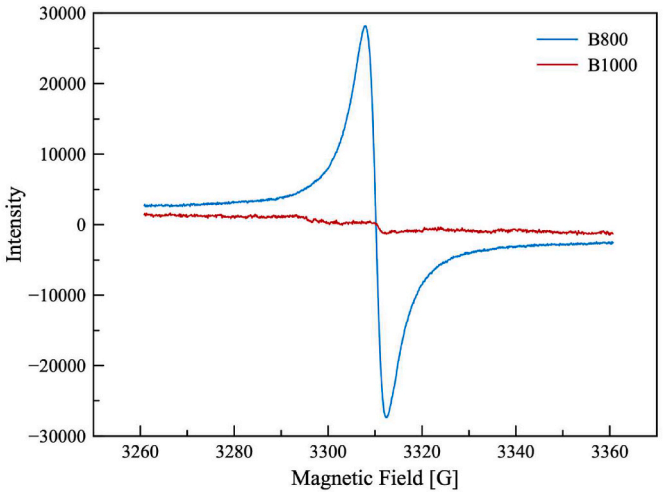

Fig. 6. EPR spectra of bamboo pyrolyzed powders.

Table 2
Concentrations, *g*-factor, and line width of PFRs in bamboo samples obtained at different pyrolysis temperatures [41].

Entry	Sample	Line Width (Gauss)	Radicals' concentration (Spins/g)[a]	*g* factor[b]
1	B800	4.37 ± 0.1	1.85×10^{18}	2.0029 ± 0.0001
2	B1000	3.10 ± 0.1	3.40×10^{15}	2.0028 ± 0.0001

[a] PFR concentration was determined by comparing the EPR signal's double integral with an external standard solution (3 mM) of tetramethyl pyperidin-*N*-oxyl radical (TEMPO).
[b] *g*-factor values were corrected against the perylene radical cation in concentrated sulphuric acid (g = 2.00258).

continues to be a subject of ongoing discussion, primarily due to the complexity inherent in their microstructure [4]. The lithium storage performance of the B800 and B1000 electrodes has been characterized using galvanostatic discharge/charge cycling and cyclic voltammetry (CV) (Fig. 8). All the electrochemical measurements were performed within the potential window of 0.01–3.0 V vs. Li^+/Li.

The CV profiles obtained for both negative electrodes during the initial and subsequent cycles are shown in Fig. 8a. For the B800 electrode, during the first reduction process, the weak and prominent cathodic peaks, respectively, at 1,45 V and 0.75 V, are observed during the first cathodic scan. Both are attributed to the irreversible reactions between the electrolyte and surface functional groups (high specific surface area of the bamboo biochar material), namely, the solid electrolyte interphase (SEI) formation [26]. The two CV have a similar shape to a previously reported article in which ivy-based biochar was used as anode in lithium-ion batteries [63], where the authors calculated the contribution of the surface (non-faradaic current) and bulk (faradaic current) processes to the overall current. Likewise, in our case, the bulk reaction is the most dominant process. We notice that both peaks disappeared in the following cycles, which is attributed to the complete stabilization of the SEI layer during the first reduction cycle (Fig. S12). The reduction peak near 0V is related to the lithium intercalation into the graphitic carbon layers, which is repeated in the following cycling, confirming the reversible Li^+ intercalation process [51,64–66].

In contrast, B1000 shows two distinct features around 0.70 and 0.9 V during the first cycle. These characteristics can be attributed to the interfacial SEI formation process followed by lithium surface absorption phenomena [64,66]. The distinct chemical and physical characteristics of B800 and B1000, such as surface area, pore size, and PFRs, could be relevant to these observations. Conversely, the

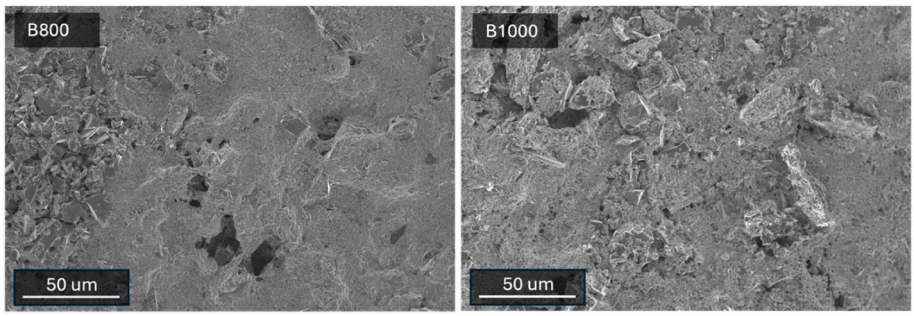

Fig. 7. SEM images of the bamboo-based slurries.

intercalation/de-intercalation peaks occur near 0.1 V, while a distinct anodic peak around 1.0 V is attributed to adsorption at heteroatoms, edges, and other sites within the carbonaceous materials [67].

To examine how both materials respond to various currents, the cells underwent charging and discharging cycles at rates ranging from C/5 to 10C, and then back to C/5. Fig. 8b shows the discharge-specific capacity as a function of the rate. The B800 electrode exhibits a significant discharge capacity of 230 mAh/g at C/5 and 50 mAh/g at 10C. In contrast, the B1000 electrode delivers a discharge capacity value of 210 mAh/g at C/5 and 95 mAh/g at 10C. However, the superior rate performance of B1000 at higher C-rates can be attributed to its well-developed hierarchical porosity as well as its higher electrical conductivity, which enables efficient ion diffusion throughout the carbon bulk from the surface to the storage active sites, including the interlayers of disordered and graphitic domains.

The galvanostatic charge/discharge (GCD) profiles and extended cycling test at C/5 after activation cycles (low current rate of C/20 used during the first three cycles), respectively, are shown in Fig. 8c–e. The GCD profiles of both biochar materials consist of two distinct steps: a sloping region extending to approximately 0.1 V, followed by a low potential plateau (Fig. 8c and d). These characteristics are well-described by the adsorption-intercalation model, which explains the same features observed previously in the CV curves [68]. As observed, the B800 anode delivers a higher reversible discharge capacity of 230 mAh/g, at C/5, which is slightly higher than that of the B1000 anode (200 mAh/g). Both anodes exhibit an excellent capacity retention of 100 % after 450 cycles.

Nonetheless, the B800 anode also exhibits a higher initial Coulombic efficiency (ICE) of 69 %, compared to an ICE of 52 % for the B1000 anode. The higher specific capacity of B800 can be attributed to its larger surface area (310 m^2/g) and smaller pore size (38 A), as demonstrated by BET measurements (Fig. 5). These characteristics reduce diffusion pathways within the graphite interlayers and through the defects. Additionally, the higher ICE of B800 can be linked to a more uniform particle distribution and less aggregation, as SEM shows less interaction between the pores and the electrolyte interior. However, an appropriate increase in carbonization temperature generally decreases the BET-specific surface area (B1000) [69]. This increase in temperature is beneficial for enlarging the closed pore volume and long stripes, thereby promoting higher conductivity, which explains the improved performance at high C-rates as well.

Table 3 summarizes previous research on biochar derived from bamboo and other woods as active materials for negative electrodes in LIBs. As observed, the material under discussion exhibits a lower capacity than those presented in the table. However, it is noteworthy that this material is the only one that has not undergone any chemical treatment or activation procedures, making it highly economical and appealing from an industrial perspective. Additionally, the specific capacity of B800 remains stable even after 400 cycles, while B1000 shows a slight increase, which is an unusual and positive phenomenon compared to the other materials reported. Finally, the temperature employed is consistent with the temperatures in other studies, and the coulombic efficiency is highly satisfactory. Further investigation into this material is necessary. Potential research avenues include studying its performance in sodium-ion batteries (SIBs) and exploring the effects of implementing a minimally invasive and cost-effective pre-treatment on the material.

4. Conclusion

We were motivated to develop a carbon anode for lithium batteries using bamboo-based biochar as raw material without any chemical or physical treatment. We disclosed a sustainable, low-cost production of conductive carbons by slow-pyrolysis of the *Dendrocalamus giganteus* bamboo species.

This study demonstrates the significant potential of bamboo-based biochars (BCs) as sustainable and efficient anode materials for lithium-ion batteries (LIBs). The B800 biochar, prepared through slow pyrolysis at 800 °C, exhibited superior physicochemical properties compared to B1000, including higher d-spacing, larger graphitic crystallite size, smaller pore sizes with a higher surface area, and a greater concentration of paramagnetic aromatic π-radicals (persistent free radical-PFR). These attributes contributed to improved lithiation and reduction processes, resulting in a high reversible capacity of approximately 250 mAh/g and excellent long-term stability up to 450 cycles. The production of these greener BCs without chemical and physical pre- and post-treatments further underscores their environmental and economic advantages. Therefore, bamboo-based biochar presents a promising avenue for developing greener, cost-effective, and high-performance anodes for the next generation of LIBs, aligning with the broader goals of sustainability and efficiency in energy storage technologies.

CRediT authorship contribution statement

Mario J. Barbosa Nogueira: Writing – review & editing, Writing – original draft, Visualization, Methodology, Formal analysis, Data curation. **Susana Chauque:** Writing – review & editing, Writing – original draft, Formal analysis, Data curation. **Valeria Sperati:** Writing – review & editing, Writing – original draft, Formal analysis, Data curation. **Letizia Savio:** Writing – review & editing, Writing – original draft, Visualization, Formal analysis, Data curation. **Giorgio Divitini:** Writing – review & editing, Writing – original draft, Investigation, Formal analysis, Data curation. **Lea Pasquale:** Writing – original draft, Investigation, Formal analysis, Data curation. **Sergio Marras:** Writing – original draft, Visualization, Formal analysis, Data curation. **Paola Franchi:** Writing – review & editing, Writing – original draft, Investigation, Formal analysis, Data curation. **Sidnei Paciornik:** Writing – review & editing, Writing – original draft, Supervision, Funding acquisition, Conceptualization. **Remo Proietti Zaccaria:** Writing – review & editing, Writing – original draft, Methodology, Investigation, Conceptualization. **Omar Ginoble Pandoli:** Writing – review & editing, Writing – original draft, Visualization, Supervision, Project

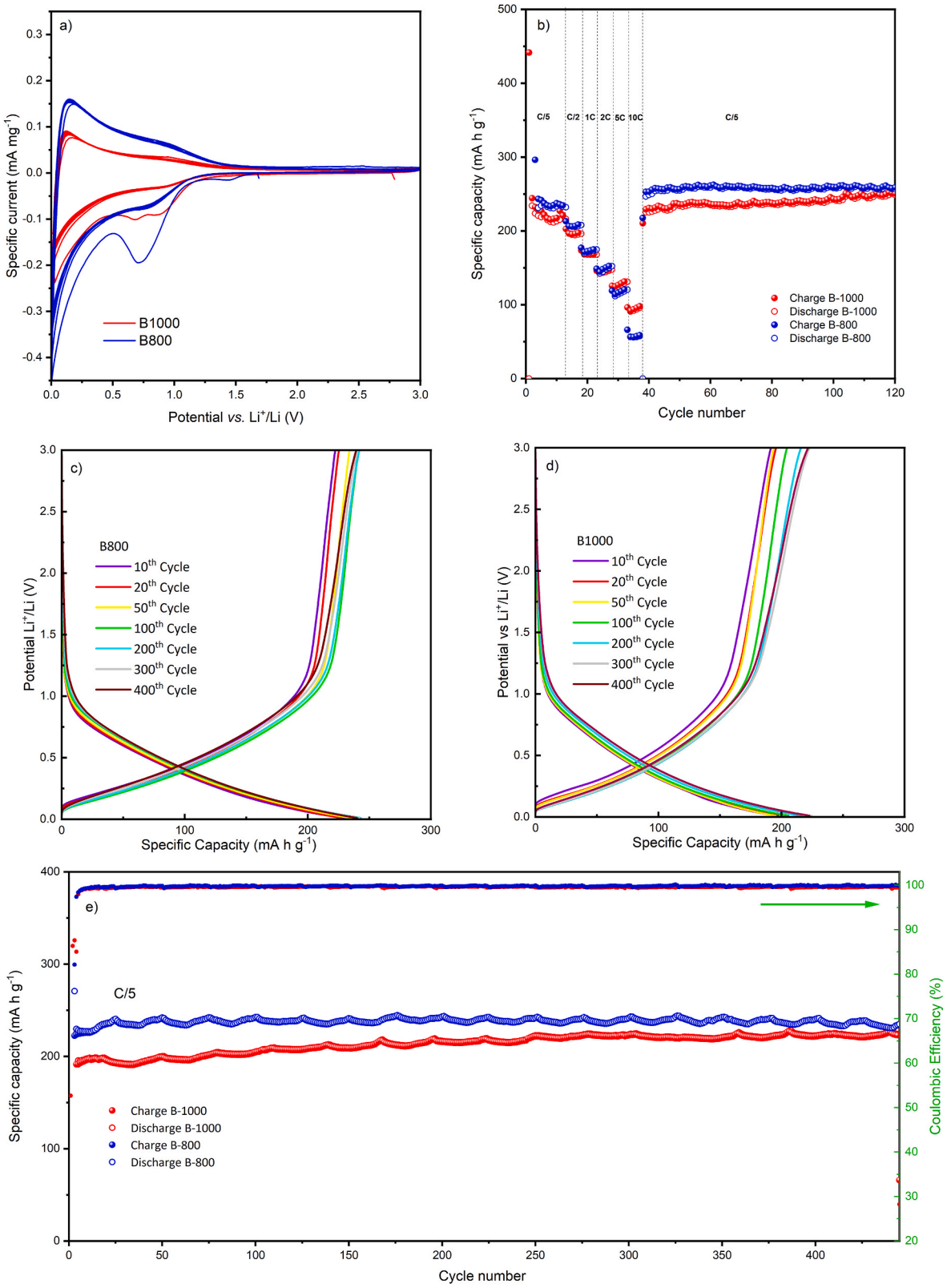

Fig. 8. Electrochemical performances of biochar anodes in LP30 as electrolyte within a potential range of 0.01–3 V at room temperature. (a) CV curves obtained, scan rate 0.05 mV/s; (b) Rate capability from C/5 to 10C and back to C/5; (c,d) Galvanostatic discharge/charge profiles at C/5; (e) Cycling performance up to 450 cycles at C/5.

Table 3
Electrochemical performance of bamboo-derived hard carbon anodes in LIB half cells – HCs produced by carbonization at relatively low temperature and chemical/physical treatment.

Biomass precursor	Pyrolysis Temp. (°C)	Chemical Agents and activation procedure	Cycle	Coulombic efficiency (%)	Current density (A g^{-1})	Capacity (mA h g^{-1})	Ref
Bamboo charcoal	MW at 900 W	Biomass was soaked in concentrated HNO_3 and HF for 12 h and then mixed with 4g of KOH	100	46 %–97 % Not reversible capacity	1	From 916 to 700 (after 100 cycles)	[21]
Carbon fiber from bamboo chopstick	at 800 °C	Hydrothermal delignification with KOH and integration with MnO_2 NPs	300	>98	0.2	710 (Pristine carbon fiber 250)	[24]
Bamboo carbon fiber	1000	Bulk bamboo was stirred in 100 ml 30 wt% HNO_3 at 80 °C for 4h.	100	>98	0.5	From 211 to 116	[25]
Bamboo Leaf's	800	Hummers' method to prepare GO from natural graphite flakes thermally treated at 800 °C under Ar/H_2 for 3h to produce Si-NP-RGO nanocomposites.	100	>98	0.2	1700	[26]
Bamboo carbon fiber	700	H_2SO_4 Composites BCF@SnO_2	100	>98	0.1	627 (Pristine carbon fiber 250)	[27]
Bamboo Charcoal	700	HCl treatment and calcination with polyacrylontrile (PAN) to obtain Si@N/C Composites	120	>98	0,2	750	[29]
Bamboo biochar	800	No chemical or physical activation	450	>98	1 0.2	175 250	This work
Bamboo biochar	1000	No chemical or physical activation	450	>98	1	165	This work

administration, Methodology, Investigation, Funding acquisition, Data curation, Conceptualization.

Acknowledgments

This work was funded with financial support of Conselho Nacional de Desenvolvimento Científico e Tecnologico-Brasil (CNPq) (458302/2013–9), Fundação Carlos Chagas Filho Amparo à Pesquisa do Estado do Rio de Janeiro (FAPERJ) (E-26/010.001646/2019, E-26/010.000980/2019 and SEI-260003/001227/2020), Coordenação de Aperfeiçoamento de Pessoal de Nível Superior – Brasil (CAPES) – Finance Code 001, Project Capes-PRINT and the European Union—Next Generation EU-the Italian Ministry of University and Research (MUR) (PRIN2022, project n. 2022JM3LZ3_(SUST-CARB)). LS acknowledges funding from the European Union – NextGenerationEU through the Italian Ministry of University and Research under project PRIN-PNRR P20227XSAH. We are thankful for the access to the facilities and equipment of the professors Tatiana Saint'Pierre (PUC-RIO) and Roberto Spotorno (UNIGE). Maurício Dupim for assistance during the ICP-EOS.

Open Access publishing facilitated by University degli Studi di Genova, as part of the CRUI-CARE agreement.

Appendix A. Supplementary data

Supplementary data to this article can be found online at https://doi.org/10.1016/j.biombioe.2024.107511.

Data availability

I have shared all the data in to the attached files

References

[1] S. Kane, A. Storer, W. Xu, C. Ryan, N.P. Stadie, Biochar as a renewable substitute for carbon black in lithium-ion battery electrodes, ACS Sustain. Chem. Eng. 10 (2022) 12226–12233, https://doi.org/10.1021/acssuschemeng.2c02974.
[2] D. Alvira, D. Antorán, J.J. Manyà, Plant-derived hard carbon as anode for sodium-ion batteries: a comprehensive review to guide interdisciplinary research, Chem. Eng. J. 447 (2022), https://doi.org/10.1016/j.cej.2022.137468.
[3] X. Yuan, B. Zhu, J. Feng, C. Wang, X. Cai, R. Qin, Recent advance of biomass-derived carbon as anode for sustainable potassium ion battery, Chem. Eng. J. 405 (2021), https://doi.org/10.1016/j.cej.2020.126897.
[4] S. Alvin, H.S. Cahyadi, J. Hwang, W. Chang, S.K. Kwak, J. Kim, Revealing the intercalation mechanisms of lithium, sodium, and potassium in hard carbon, Adv. Energy Mater. 10 (2020), https://doi.org/10.1002/aenm.202000283.
[5] N. Sick, O. Krätzig, G.G. Eshetu, E. Figgemeier, A review of the publication and patent landscape of anode materials for lithium ion batteries, J. Energy Storage 43 (2021), https://doi.org/10.1016/j.est.2021.103231.
[6] D.S. Oyebamiji, D. Chandran, R. Raviadaran, Advancements in electrochemical energy storage: a review of biomass-derived anode and cathode for electric vehicles battery, Biomass Bioenergy 189 (2024) 107348, https://doi.org/10.1016/j.biombioe.2024.107348.
[7] G.N. Newton, L.R. Johnson, D.A. Walsh, B.J. Hwang, H. Han, Sustainability of battery technologies: today and tomorrow, ACS Sustain. Chem. Eng. 9 (2021) 6507–6509, https://doi.org/10.1021/acssuschemeng.1c02909.
[8] A. Prévoteau, F. Ronsse, I. Cid, P. Boeckx, K. Rabaey, The electron donating capacity of biochar is dramatically underestimated, Sci. Rep. 6 (2016), https://doi.org/10.1038/srep32870.
[9] J. Yuan, Y. Wen, D.D. Dionysiou, V.K. Sharma, X. Ma, Biochar as a novel carbon-negative electron source and mediator: electron exchange capacity (EEC) and environmentally persistent free radicals (EPFRs): a review, Chem. Eng. J. 429 (2022), https://doi.org/10.1016/j.cej.2021.132313.
[10] L. Klüpfel, M. Keiluweit, M. Kleber, M. Sander, Redox properties of plant biomass-derived black carbon (biochar), Environ. Sci. Technol. 48 (2014) 5601–5611, https://doi.org/10.1021/es500906d.
[11] J.M.O. Scurlock, D.C. Dayton, B. Hames, Bamboo: an overlooked biomass resource? Biomass Bioenergy 19 (2000) 229–244, https://doi.org/10.1016/S0961-9534(00)00038-6.
[12] Z. Liu, Y. Zhu, D. Jiao, Z. Weng, Z. Zhang, R.O. Ritchie, Enhanced protective role in materials with gradient structural orientations: lessons from Nature, Acta Biomater. 44 (2016) 31–40, https://doi.org/10.1016/j.actbio.2016.08.005.
[13] Z. Liu, M.A. Meyers, Z. Zhang, R.O. Ritchie, Functional gradients and heterogeneities in biological materials: design principles, functions, and bioinspired applications, Prog. Mater. Sci. 88 (2017) 467–498, https://doi.org/10.1016/j.pmatsci.2017.04.013.
[14] Q. Lin, R. Gao, D. Li, Y. Lu, S. Liu, Y. Yu, Y. Huang, W. Yu, Bamboo-inspired cell-scale assembly for energy device applications, Npj Flex. Electron. 6 (2022), https://doi.org/10.1038/s41528-022-00148-w.
[15] Y. Gong, D. Li, C. Luo, Q. Fu, C. Pan, Highly porous graphitic biomass carbon as advanced electrode materials for supercapacitors, Green Chem. 19 (2017) 4132–4140, https://doi.org/10.1039/c7gc01681f.
[16] M. Fujishige, I. Yoshida, Y. Toya, Y. Banba, K. ichi Oshida, Y. suke Tanaka, P. Dulyaseree, W. Wongwiriyapan, K. Takeuchi, Preparation of activated carbon from bamboo-cellulose fiber and its use for EDLC electrode material, J. Environ. Chem. Eng. 5 (2017) 1801–1808, https://doi.org/10.1016/j.jece.2017.03.011.
[17] J. Li, Q. Wu, Water bamboo-derived porous carbons as electrode materials for supercapacitors, New J. Chem. 39 (2015) 3859–3864, https://doi.org/10.1039/c4nj01853b.
[18] G. Zhang, Y. Chen, Y. Chen, H. Guo, Activated biomass carbon made from bamboo as electrode material for supercapacitors, Mater. Res. Bull. 102 (2018) 391–398, https://doi.org/10.1016/j.materresbull.2018.03.006.
[19] Q. Wang, Y. Zhang, H. Jiang, T. Hu, C. Meng, In situ generated Ni3Si2O5(OH)4 on mesoporous heteroatom-enriched carbon derived from natural bamboo leaves for high-performance supercapacitors, ACS Appl. Energy Mater. 1 (2018) 3396–3409, https://doi.org/10.1021/acsaem.8b00556.
[20] K. Zhu, Z. Lu, S. Cong, G. Cheng, P. Ma, Y. Lou, J. Ding, N. Yuan, M.H. Rümmeli, G. Zou, Ultraflexible and lightweight bamboo-derived transparent electrodes for perovskite solar cells, Small 15 (2019), https://doi.org/10.1002/smll.201902878.

[21] R. Su, X. Dong, Preparation and electrochemical properties of bamboo-based carbon for lithium-ion-battery anode material, Int. J. Electrochem. Sci. 14 (2019) 2452–2461, https://doi.org/10.20964/2019.03.50.
[22] X. Gu, C. Lai, F. Liu, W. Yang, Y. Hou, S. Zhang, A conductive interwoven bamboo carbon fiber membrane for Li-S batteries, J. Mater. Chem. A Mater. 3 (2015) 9502–9509, https://doi.org/10.1039/c5ta00681c.
[23] DrP. Patil, A. Mhaskar, G. Kalyankar, D. Garg, Green anodes by bamboo based material for lithium-ion batteries: a review, Int. J. Adv. Res. Sci., Commun.Technol. (2021) 759–764, https://doi.org/10.48175/ijarsct-1026.
[24] J. Jiang, J. Zhu, W. Ai, Z. Fan, X. Shen, C. Zou, J. Liu, H. Zhang, T. Yu, Evolution of disposable bamboo chopsticks into uniform carbon fibers: a smart strategy to fabricate sustainable anodes for Li-ion batteries, Energy Environ. Sci. 7 (2014) 2670–2679, https://doi.org/10.1039/c4ee00602j.
[25] X. Zhang, J. Hu, X. Chen, M. Zhang, Q. Huang, X. Du, Y. Liu, X. Li, Microtubular carbon fibers derived from bamboo and wood as sustainable anodes for lithium and sodium ion batteries, J. Porous Mater. 26 (2019) 1821–1830, https://doi.org/10.1007/s10934-019-00781-3.
[26] L. Wang, B. Gao, C. Peng, X. Peng, J. Fu, P.K. Chu, K. Huo, Bamboo leaf derived ultrafine Si nanoparticles and Si/C nanocomposites for high-performance Li-ion battery anodes, Nanoscale 7 (2015) 13840–13847, https://doi.org/10.1039/c5nr02578h.
[27] Q. Han, Z. Yi, F. Wang, Y. Wu, L. Wang, Preparation of bamboo carbon fiber and sandwich-like bamboo carbon fiber@SnO2@carbon composites and their potential application in structural lithium-ion battery anodes, J. Alloys Compd. 709 (2017) 227–233, https://doi.org/10.1016/j.jallcom.2017.03.141.
[28] T. Xu, X. Qiu, X. Zhang, Y. Xia, Regulation of surface oxygen functional groups and pore structure of bamboo-derived hard carbon for enhanced sodium storage performance, Chem. Eng. J. 452 (2023), https://doi.org/10.1016/j.cej.2022.139514.
[29] C. Zhang, X. Cai, W. Chen, S. Yang, D. Xu, Y. Fang, X. Yu, 3D porous silicon/N-doped carbon composite derived from bamboo charcoal as high-performance anode material for lithium-ion batteries, ACS Sustain. Chem. Eng. 6 (2018) 9930–9939, https://doi.org/10.1021/acssuschemeng.8b01189.
[30] F. Nogata, H. Takahashi, Intelligent functionally graded material: bamboo, Compos. Eng. 5 (1995) 743–751, https://doi.org/10.1016/0961-9526(95)00037-N.
[31] A. Azadeh, K. Ghavami, The influence of heat on shrinkage and water absorption of Dendrocalamus giganteus bamboo as a functionally graded material, Construct. Build. Mater. 186 (2018) 145–154, https://doi.org/10.1016/j.conbuildmat.2018.07.011.
[32] P.S. Ghavami K, C.S. Rodrigues, Bamboo functionally graded composite material, Asian J. Civ. Eng. 4 (2003) 1–10.
[33] H. Sun, X. Li, H. Li, D. Hui, M. Gaff, R. Lorenzo, Nanotechnology application on bamboo materials: a review, Nanotechnol. Rev. 11 (2022) 1670–1695, https://doi.org/10.1515/ntrev-2022-0101.
[34] O. Ginoble Pandoli, S. Paciornik, M. Strauss, M. Santhiago, Bamboo-based microfluidic system for sustainable bio-devices, in: Environmental Footprints and Eco-Design of Products and Processes, Springer, 2022, pp. 141–169, https://doi.org/10.1007/978-981-19-1812-4_6.
[35] O. Ginoble Pandoli, Heterogeneous flow chemistry through bamboo-based microfluidic reactors, Tetrahedron. Green Chem. 2 (2023) 100022, https://doi.org/10.1016/j.tgchem.2023.100022.
[36] D.S. De Sá, R. De Andrade Bustamante, C.E. Rodrigues Rocha, V.D. Da Silva, E. J. Da Rocha Rodrigues, C. Djenne Buarque Müller, K. Ghavami, A. Massi, O. Ginoble Pandoli, Fabrication of lignocellulose-based microreactors: copper-functionalized bamboo for continuous-flow CuAAC click reactions, ACS Sustain. Chem. Eng. 7 (2019) 3267–3273, https://doi.org/10.1021/acssuschemeng.8b05273.
[37] O.G. Pandoli, R.J.G. Neto, N.R. Oliveira, A.C. Fingolo, C.C. Corrêa, K. Ghavami, M. Strauss, M. Santhiago, Ultra-highly conductive hollow channels guided by a bamboo bio-template for electric and electrochemical devices, J. Mater. Chem. A Mater. 8 (2020) 4030–4039, https://doi.org/10.1039/C9TA13069A.
[38] O. Ginoble Pandoli, R.S. Martins, K.L.G. De Toni, S. Paciornik, M.H.P. Maurício, R. M.C. Lima, N.B. Padilha, S. Letichevsky, R.R. Avillez, E.J.R. Rodrigues, K. Ghavami, A regioselective coating onto microarray channels of bamboo with chitosan-based silver nanoparticles, J. Coating Technol. Res. 16 (2019) 999–1011, https://doi.org/10.1007/s11998-018-00175-1.
[39] E.J. da Rocha Rodrigues, R. Pinto Cucinelli Neto, H. Diniz Lopes Alves, S. Paciornik, D. Santos de Sá, K. Ghavami, O. Ginoble Pandoli, An investigation of the fluid-holding cavities in a lignocellulose-based bamboo matrix via a combined X-ray microtomography and proton time-domain NMR approach, Cellul. (2023), https://doi.org/10.1007/s10570-023-05197-6.
[40] L.O.L. Gontijo, M.N. Barbosa Junior, D. Santos de Sá, S. Letichevsky, M.J. Pedrozo-Peñafiel, R.Q. Aucélio, I.S. Bott, H. Diniz Lopes Alves, B. Fragneaud, I. Oliveira Maciel, A. Linhares Rossi, L. Savio, G. Carraro, D. Anja, F. Lazaro Freire, G. Khosrow, S. Paciornik, O. Ginoble Pandoli, 3D conductive monolithic carbons from pyrolyzed bamboo for microfluidic self-heating system, Carbon N Y (2023) 118214, https://doi.org/10.1016/j.carbon.2023.118214.
[41] F. Zanardi, F. Romei, M. Nogueira Barbosa Junior, S. Paciornik, P. Franchi, M. Lucarini, A. Turchetti, L. Poletti, S. Alfei, O. Ginoble Pandoli, Pivotal contribute of EPR-characterized persistent free radicals in the methylene blue removal by a bamboo-based biochar-packed column flow system, ChemCatChem (2024), https://doi.org/10.1002/cctc.202401042.
[42] D.S. de Sá, E.J. da Rocha Rodrigues, N.M. Suguihiro, A.G. da Veiga, S. Paciornik, A. Massi, O. Ginoble Pandoli, One-pot synthesis of carboxymethylcellulose-templated copper-NPs for heterocatalytic huisgen-click reactions on lignocellulosic bamboo slices, Catal. Lett. 152 (2022) 3558–3575, https://doi.org/10.1007/s10562-022-03923-6.
[43] B.G. Palma, R.A.C. Leão, R.O.M.A. de Souza, O.G. Pandoli, Immobilization of lipases on lignocellulosic bamboo powder for biocatalytic transformations in batch and continuous flow, Catal. Today 381 (2021) 280–287, https://doi.org/10.1016/j.cattod.2020.04.041.
[44] D.S. de Sá, R. de Andrade Bustamante, C.E. Rodrigues Rocha, V.D. da Silva, E.J. da Rocha Rodrigues, C. Djenne Buarque Müller, K. Ghavami, A. Massi, O. Ginoble Pandoli, Fabrication of lignocellulose-based microreactors: copper-functionalized bamboo for continuous-flow CuAAC click reactions, ACS Sustain. Chem. Eng. 7 (2019) 3267–3273, https://doi.org/10.1021/acssuschemeng.8b05273.
[45] R. Spotorno, M. Ostrowska, S. Delsante, U. Dahlmann, P. Piccardo, Characterization of glass-ceramic sealant for solid oxide fuel cells at operating conditions by electrochemical impedance spectroscopy, Mater. 13 (2020) 1–13, https://doi.org/10.3390/ma13214702.
[46] A. Nikitin, L.-Å. Näslund, Z. Zhang, A. Nilsson, C–H bond formation at the graphite surface studied with core level spectroscopy, Surf. Sci. 602 (2008) 2575–2580, https://doi.org/10.1016/j.susc.2008.06.012.
[47] H. Yu, C. Gui, Y. Ji, X. Li, F. Rao, W. Huan, L. Li, Changes in chemical and thermal properties of bamboo after delignification treatment, Polym. 14 (2022) 2573, https://doi.org/10.3390/polym14132573.
[48] F. Meng, Y. Yu, Y. Zhang, W. Yu, J. Gao, Surface chemical composition analysis of heat-treated bamboo, Appl. Surf. Sci. 371 (2016) 383–390, https://doi.org/10.1016/j.apsusc.2016.03.015.
[49] J.F.; S.W.F.; S.P.E., B.K.D. Moulder, Handbook of X Ray Photoelectron Spectroscopy: A Reference Book of Standard Spectra for Identification and Interpretation of XPS Data, 1995.
[50] H. Darjazi, L. Bottoni, H.R. Moazami, S.J. Rezvani, L. Balducci, L. Sbrascini, A. Staffolani, A. Tombesi, F. Nobili, From waste to resources: transforming olive leaves to hard carbon as sustainable and versatile electrode material for Li/Na-ion batteries and supercapacitors, Mater. Today Sustain. 21 (2023) 100313, https://doi.org/10.1016/j.mtsust.2022.100313.
[51] H. Darjazi, A. Staffolani, L. Sbrascini, L. Bottoni, R. Tossici, F. Nobili, Sustainable anodes for lithium- and sodium-ion batteries based on coffee ground-derived hard carbon and green binders, Energies 13 (2020), https://doi.org/10.3390/en13236216.
[52] Y.-R. Rhim, D. Zhang, D.H. Fairbrother, K.A. Wepasnick, K.J. Livi, R.J. Bodnar, D. C. Nagle, Changes in electrical and microstructural properties of microcrystalline cellulose as function of carbonization temperature, Carbon N Y 48 (2010) 1012–1024, https://doi.org/10.1016/j.carbon.2009.11.020.
[53] G. Wei, J. Yu, M. Gu, T.B. Tang, Dielectric relaxation and hopping conduction in reduced graphite oxide, J. Appl. Phys. 119 (2016), https://doi.org/10.1063/1.4953357.
[54] M. Mohandoss, S. Sen Gupta, A. Nelleri, T. Pradeep, S.M. Maliyekkal, Solar mediated reduction of graphene oxide, RSC Adv. 7 (2017) 957–963, https://doi.org/10.1039/C6RA24696F.
[55] G.G. Politano, C. Versace, Recent advances in the Raman investigation of structural and optical properties of graphene and other two-dimensional materials, Cryst. 13 (2023) 1357, https://doi.org/10.3390/cryst13091357.
[56] D. Zhan, Z. Ni, W. Chen, L. Sun, Z. Luo, L. Lai, T. Yu, A.T.S. Wee, Z. Shen, Electronic structure of graphite oxide and thermally reduced graphite oxide, Carbon N Y 49 (2011) 1362–1366, https://doi.org/10.1016/j.carbon.2010.12.002.
[57] Y. Wang, X. Gu, Y. Huang, Z. Ding, Y. Chen, X. Hu, Insight into biomass feedstock on formation of biochar-bound environmentally persistent free radicals under different pyrolysis temperatures, RSC Adv. 12 (2022) 19318–19326, https://doi.org/10.1039/d2ra03052g.
[58] E.G. Marina Brustolon, Electron Paramagnetic Resonance, Wiley, 2009, https://doi.org/10.1002/9780470432235.
[59] E. Zhecheva, R. Stoyanova, J.M. Jiménez-Mateos, R. Alcántara, P. Lavela, J. L. Tirado, EPR study on petroleum cokes annealed at different temperatures and used in lithium and sodium batteries, Carbon N Y 40 (2002) 2301–2306, https://doi.org/10.1016/S0008-6223(02)00121-5.
[60] R. Kukeva, M. Kalapsazova, H. Rasheev, G. Vassilev, A. Tadjer, R. Stoyanova, In situ electron paramagnetic resonance monitoring of predegradation radical generation in a lithium electrolyte, J. Phys. Chem. Lett. 14 (2023) 9633–9639, https://doi.org/10.1021/acs.jpclett.3c02374.
[61] X. Sang, X. Xu, Z. Bu, S. Zhai, Y. Sun, M. Ruan, Q. Li, Application of electron paramagnetic resonance in an electrochemical energy storage system, Magnetochem. 9 (2023), https://doi.org/10.3390/magnetochemistry9030063.
[62] B. Wang, W. Wang, K. Sun, Y. Xu, Y. Sun, Q. Li, H. Hu, M. Wu, Developing in situ electron paramagnetic resonance characterization for understanding electron transfer of rechargeable batteries, Nano Res. 16 (2023) 11992–12012, https://doi.org/10.1007/s12274-023-5855-z.
[63] P. Salimi, W. Vercruysse, S. Chauque, S. Yari, E. Venezia, A. Lataf, N. Ghanemnia, M.S. Zafar, M. Safari, A. Hardy, R. Proietti Zaccaria, D. Vandamme, Lithium-metal-free sulfur batteries with biochar and steam-activated biochar-based anodes from spent common ivy, Energy & Environ. Mater. 7 (2024), https://doi.org/10.1002/eem2.12758.
[64] M. Winter, J.O. Besenhard, Lithiated carbons, in: Handbook of Battery Materials, Wiley, 2011, pp. 433–478, https://doi.org/10.1002/9783527637188.ch15.
[65] K. Wang, Y. Xu, H. Wu, R. Yuan, M. Zong, Y. Li, V. Dravid, W. Ai, J. Wu, A hybrid lithium storage mechanism of hard carbon enhances its performance as anodes for lithium-ion batteries, Carbon N Y 178 (2021) 443–450, https://doi.org/10.1016/j.carbon.2020.11.095.

[66] Y. Huang, Y. Wang, P. Bai, Y. Xu, Storage mechanism of alkali metal ions in the hard carbon anode: an electrochemical viewpoint, ACS Appl. Mater. Interfac. 13 (2021) 38441–38449, https://doi.org/10.1021/acsami.1c12150.
[67] Y. Huang, Y. Wang, P. Bai, Y. Xu, Storage mechanism of alkali metal ions in the hard carbon anode: an electrochemical viewpoint, ACS Appl. Mater. Interfac. 13 (2021) 38441–38449, https://doi.org/10.1021/acsami.1c12150.
[68] U. Ghani, N. Iqbal, A.A. Aboalhassan, B. Liu, T. Aftab, I. Zada, F. Ullah, J. Gu, Y. Li, S. Zhu, Q. Liu, One-step sonochemical fabrication of biomass-derived porous hard carbons; towards tuned-surface anodes of sodium-ion batteries, J. Colloid Interfac. Sci. 611 (2022) 578–587, https://doi.org/10.1016/j.jcis.2021.12.104.
[69] A.K. Kercher, D.C. Nagle, M Icrostructural Evolution during Charcoal Carbonization by X-Ray Diffraction Analysis, 2003.